

Assessing LAPAN-A3 Satellite with Line Imager Space Application (LISA) Sensor for Oil Spill Detection

Pingkan Mayestika Afgatiani^{a,*}, Andi Ibrahim^a, Maryani Hartuti^a, Ega Asti Anggari^b, Agus Herawan^b, Patria Rachman Hakim^b, Ety Parwati^a

^a Research Center for Remote Sensing, National Research and Innovation Agency (BRIN), Jakarta, 13710, Indonesia

^b Research Center for Satellite Technology, National Research and Innovation Agency (BRIN), Bogor, 16310, Indonesia

Corresponding author: *pingkan.mayestika.afgatiani@brin.go.id

Abstract— LAPAN-A3 (LA3) data has been utilized for earth observation in monitoring natural resources. While most applications are toward land resources monitoring, recent utilization indicates the possibility of LA3 detecting oil spill events on the sea surface. This research provides information regarding the ability of sensors characteristics of LA3 to detect oil slicks and its initial results by examining multispectral bands combination using Optimum Index Factor (OIF), and Digital Number (DN) extraction is carried out on each LA3 band in water-oil-water since LA3 is not able to change DN to reflectance value. In this study, besides using LA3 data, Sentinel-2 data was also used as comparative data and results in validation. Based on the results of the OIF calculation, the combination of the Blue-Green-NIR (BGN) band has the highest value compared to other combinations. This indicates that the BGN band combination is appropriate for visualizing oil and distinguishing between oil and water. The pattern formed from the visualization results with the combination of the BGN band is silvery in crude oil and greenish in ship waste disposal. The result is also strengthened by DN extraction from slick oil samples that shows a prominent pattern on the Blue and Green bands. Finally, this study can conclude that LA3 has great potential to detect oil spills visually but still requires further research for reflectance analysis by converting the DN value into reflectance.

Keywords— Band combination; LAPAN-A3; oil slick; optical satellite; optimum index factor.

Manuscript received 16 Aug. 2021; revised 9 Jun. 2022; accepted 12 Jul. 2022. Date of publication 31 Dec. 2022.
IJASEIT is licensed under a Creative Commons Attribution-Share Alike 4.0 International License.



I. INTRODUCTION

Oil spill accidents from ships or oil platforms cause damage to marine and coastal environments and ecosystems [1]–[3]. Oil spills may be due to releases of crude oil from tankers, offshore platforms, drilling rigs, and wells, as well as spills of refined petroleum products (such as gasoline and diesel) and their by-products, heavier fuels used by large ships such as bunker fuel, or the spill of any oily refuse or waste oil [4]. Oil spills found in marine environments have different types of oil, and these can come from oil platforms, shipwrecks, oil pipeline leaks, unforeseen disasters, and land-based runoffs [5]–[7]. Efficient monitoring and early identification of oil slicks are vital for the corresponding authorities to react wisely, restrict environmental pollution and avoid further damage [8], [9].

Oil spill detection can easily be done by utilizing satellite remote sensing data such as active microwave sensors, laser floor sensors method, and optical remote sensing. Active

microwave sensors are widely used remote sensing systems for oil spill detection and monitoring because of their extensive coverage and ability to collect day and night data in all weather conditions [10]. The main radar imaging types are used for oil spill detection, namely synthetic aperture radar (SAR) and side-looking airborne radar (SLAR). The presence of oil in the ocean usually reduces the intensity of backscatter energy. As a result, in the SAR image, the oil spill looks dark. However, there are shortcomings in detecting oil spills using SAR images. Oil spills are just one of the other phenomena that can lead to them, such as man-made or natural events. It reduces the scattering mechanism and looks dark in SAR images. These phenomena are well known as a look-alike, it may include: a natural surface film produced by plankton or fish, grease, floating algae, internal waves, weak wind areas, vegetable oils, shipwrecks, and convergence zones. Meanwhile, the laser floor sensors in oil spill detection remains limited. Optical remote sensing (ORS) of reflected sunlight has been widely used to assess oil spills in the ocean

for several decades. Recent studies started using more spectral bands to obtain more information from the detected features to discard look-alikes, classify oil types, track an oil tanker collision, and/or quantify oil concentration or volume [4], [5]. However, cloud cover frequency is highly affected by ORS, especially in the rainy season [11]. This limitation is compensated by the multiple ORS sensors currently in orbit and multiband spectral data from any individual sensor [4]. ORS sensors with a visible spectrum can distinguish oil and water. In the visible region of the electromagnetic spectrum (approximately 400–700 nm), oil has a lower surface reflectance than water but shows nonspecific absorption tendencies. The reflectance of various crude oils differs depending on the type. It is explained by Hu et al. [4] that non-emulsified crude oil and oil emulsions are not visible in the narrow-band reflectance. However, the reflectance of non-emulsified crude oil decreases with increasing oil thickness.

In contrast, oil emulsions have reflectance characteristics that contrast to non-emulsified crude oil, namely a visible change in the NIR-SWIR wavelengths. Oil generally manifests throughout the entire visible spectrum. Sheen shows silvery and reflects light over a wide spectral region down to the blue [12]. Researchers have widely used the utilization of ORS imagery for oil spill detection. MODIS data were used for oil spill tracking through texture analysis [13], [14]. Landsat-8 was used for a mapping oil spill in Niger Delta by Ozigis, Kaduk, and Jarvis [15]. In other research, Arslan [16] assessed oil spills using Landsat-8 multispectral sensors in Fener (Ufak) Island, Cesme, Turkey. Kolokoussis and Karathanassi [17] and Althawadi and Hashim [18] mapped oil spills using Sentinel-2 MSI. Determination of band combination is one commonly used method for detecting oil spills. Previous studies, such as those of Kolokoussis and Karathanassi [17] and Rajendran et al. [19], used Sentinel-2 and multiple band combinations. The NIR-Red-Green band combination is commonly used in developing false-color composites (FCC), while the Red-Green-Blue band can help distinguish oil thickness

LAPAN-A3 (LA3) is the latest generation satellite belonging to Indonesia and was successfully launched in June 2016. This satellite project aims to achieve microsatellite operation in Indonesia for experimental remote sensing in agriculture and maritime traffic monitoring [20]. LA3 carries a multispectral sensor called the Line Imager Space Application (LISA). LISA is a push-broom scanner with four bands ranging from the visible (Green-Red-Blue) to near-infrared spectrum with a spatial resolution of 15 meters [21], [22], [23]. Spatial resolution around 10 – 15 meters can obtain the smaller scale oil spill onto river water, whereas the river site has complex conditions, including terrestrial [24]. So, it is absolutely possible to be utilized in ocean areas.

As the objective of LA3 utilization is for agriculture monitoring, it has been utilized to identify agricultural land and land use/land cover (LULC). The carried sensors in LA3 have the ability to present data about the seasonal agricultural

field [20]. Wijayanto, Yusuf, and Pambudi [25] assessed the capability of spectral features of LA3 to identify paddy fields in Probolinggo, East Java, and concluded that LA3 spectral features were able to detect paddy fields in the vegetative phase. LA3 is also capable of identifying LULC. In other research, Herawan et al. [26] conducted LULC classification from LA3 data over a part of Rote Island. It generated high accuracy with a small sample size in distinguishing water, bare land, agriculture, forest, and secondary forest. For further research, Arifin, Carolita, and Kartika [27] compared the NDVI model from LA3 data with Landsat-8 data for forest identification. The results showed that the NDVI range extracted from LA3 data had moderate similarity with Landsat-8. LA3 satellite data has been studied for earth observation and can be utilized for monitoring paddy fields, built-up areas, forests, agricultural lands, and bare soils [28]. It is highly possible to more explore LA3 data for other utilization purposes, such as for marine environmental monitoring.

LA3 medium-resolution multispectral data have been available for experimental purposes by the National Institute of Aeronautics and Space of Indonesia (LAPAN) since 2017. Nevertheless, its capability in oil spill detection has not yet been explored and investigated. This study aims to assess the ability of the LA3 sensor to detect oil slick and its initial results by incorporating LISA multispectral bands.

II. MATERIALS AND METHOD

A. Study Area

Fig. 1 shows the two study sites for this research: Bintan waters and Karawang waters. The first location is Bintan waters, located in the border area between Indonesia, Malaysia, and Singapore. Bintan waters are included in Riau Islands Province, located in the western hemisphere of Indonesia. It is one of the waters located on the border of the country's territory, with a relatively dense area for international shipping lanes. It is mostly traversed by passenger ships, logistic ships, tankers, barges, and container ships. The many types of ships that cross make Bintan waters vulnerable to oil spill pollution from ship activities. Oil spill events are almost found throughout the year in Bintan waters with various areas of oil slicks. This area is under surveillance and investigation by Indonesia's environmental pollution task force related to oil spill pollution. Oil spill events in this location are mostly caused by waste ship disposal onto the sea. The second study site is Karawang Waters, located in Karawang Regency, West Java, Indonesia. There are offshore oil and gas exploration activities located in Karawang waters. The offshore oil and gas well is located approximately 38 km from shore. In July 2019, one of the oil drilling rigs known YYA-1 was leaked. The leaking pipeline caused the large oil slick to begin spreading around the rig site and floated for about two months. The sea current flowed the oil slicks to shore and impacted the resident who lived near the shore.

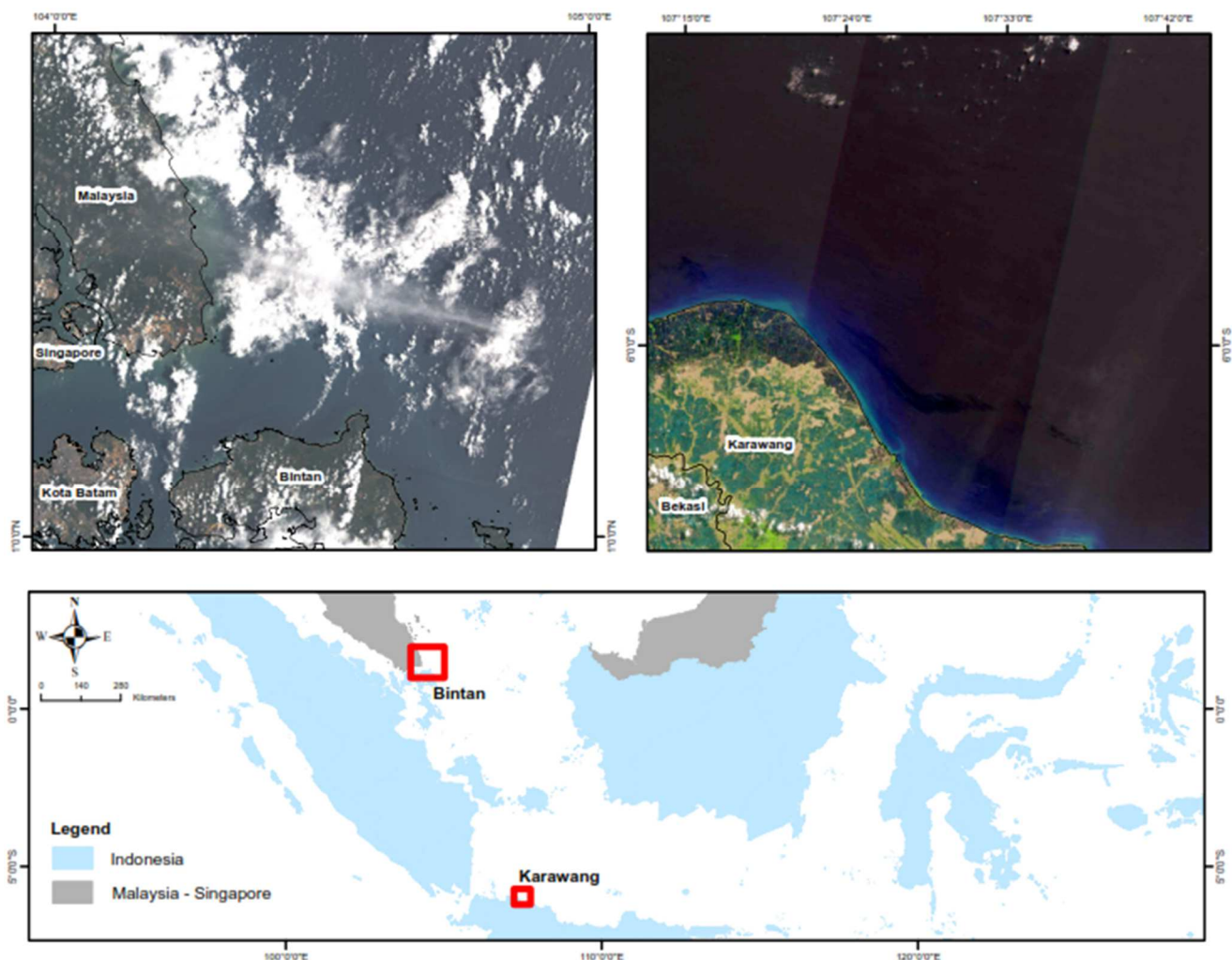


Fig. 1 Locations of study in Bintan and Karawang waters

B. Satellite Data

The LAPAN-A3 data and Sentinel-2 data were used in this study. They both are categorized into medium-resolution satellite images. The availability of 15 m LAPAN-A3 for the study was acquired from Satellite Technology Research Center, National Research and Innovation Agency (BRIN). This satellite data is currently aimed for experimental purposes related to environmental monitoring. In sun-synchronous orbit near-equatorial at about 650 or 550 km altitude above Earth's surface, the multispectral LA3 samples four spectral bands in the visible and near-infrared spectral range. Each band line's size consists of 8023 pixels; effective pixels are 6000 pixels. This line imager camera uses a 300 mm lens with an altitude of 650 km. It is expected to have ~18 m resolution with ~120 km swath of image [20]. On the other hand, Sentinel-2 data was acquired from Copernicus European. Sentinel-2A was launched on June 23, 2015, in the European Commission's Copernicus program, and two years later, Sentinel-2B was launched, on March 7, 2017, to be exact. This satellite orbits in a sun-synchronous also at a mean altitude of 786 km above Earth's surface. It carries the Multi-Spectral Imager (MSI) with 13 spectral bands, from visible-near infrared (VNIR) to shortwave infrared (SWIR) [29]. Each band has three different spatial resolutions, including 10, 20, and 60 m (Table 1).

TABLE I
OPTICAL SATELLITE BANDS

Satellite Name	Band	Spectral Range
LAPAN-A3	B1 – Blue	410 – 490 nm
	B2 – Green	510 – 580 nm
	B3 – Red	630 – 700 nm
	B4 – NIR	770 – 990 nm
Sentinel-2	B1 – Coastal Aerosol	443,9 nm (S2A) / 442,3 nm (S2B)
	B2 – Blue	496,6 nm (S2A) / 492,1nm (S2B)
	B3 – Green	560 nm (S2A) / 559nm (S2B)
	B4 – Red	664,5 nm (S2A) / 665 nm (S2B)
	B5 – Vegetation Red Edge 1	703,9 nm (S2A) / 703,8 nm (S2B)
	B6 – Vegetation Red Edge 2	740,2 nm (S2A) / 739,1 nm (S2B)
	B7 – Vegetation Red Edge 3	782,5 nm (S2A) / 779,7 nm (S2B)
	B8 – NIR	835,1 nm (S2A) / 833 nm (S2B)
	B8A – Narrow NIR	864,8 nm (S2A) / 864nm (S2B)
	B9 – Water Vapour	945 nm (S2A) / 943,2 nm (S2B)

B10 – SWIR-Cirrus	1373,5 nm (S2A) / 1376,9 nm (S2B)
B11 – SWIR	1613,7 nm (S2A) / 1610,4 nm (S2B)
B12 – SWIR	2202,4 nm (S2A) / 2185,7 nm (S2B)

This study processed and analyzed LAPAN-A3 data as the main research object and Sentinel-2 data as the comparison feature to assess the ability of LA3 in oil spill detection. Two images of LAPAN-A3 used in this study were sensed on February 27, 2021, at 01:49 am UTC in Bintan waters and August 14, 2019, at 02:09 am UTC in Karawang waters. Meanwhile, Sentinel-2 was used to compare the result of oil spill detection from LAPAN-A3, which were sensed on February 26, 2021, at 03:07 am UTC in Bintan waters and August 13, 2019, at 02:55 am UTC in Karawang waters. Level 2A Surface Reflectance data of Sentinel-2 were selected for further analysis in this study. The two images are compared according to their respective locations as it contains the study site.

C. Research Stages

Generally, the method used in this study uses visual interpretation by developing a color composite to enhance the oil spill features. Specifically, there are three main stages of the research method in this study that are conducted to achieve the research objectives. Those are pre-processing satellite data, processing satellite data, and post-processing. The proposed method used is presented in Fig. 2.

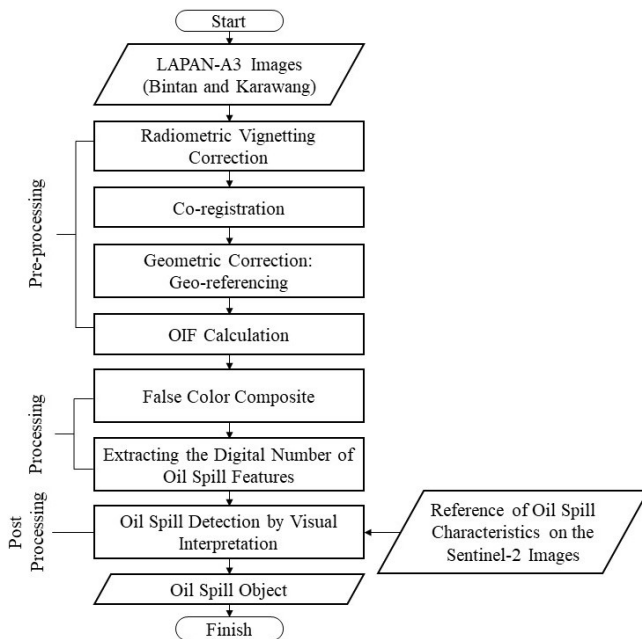


Fig. 2 The stages of the method in this study

D. Satellite Image Pre-processing

Image pre-processing is required to correct radiometric and geometric distortions. There are three processes in LA3 image pre-processing: Radiometric Vignetting Correction, Band Co-Registration, and Direct Geo-referencing for geometric correction. Radiometric vignetting correction is performed to eliminate the vignetting effect. Vignetting effect causes differences in brightness at the center and edges of the image.

The vignetting effect was reduced from 40% to 10% after correcting for the relative digital number [30].

Band Co-Registration is done due to distortion where the object in the image of one band does not align with the object in the image of another band. As a result of this distortion, the image will appear blurry (blurry effect). In the LA3 co-registration band correction using the image correction method (image matching). The image on the red band is used as a reference, while the image on the NGB band will merge into the red band image [31].

Direct geo-referencing is used to determine the coordinates of the earth image. Image with good geometry if in the process of image capture, the camera and satellite movements are in stable condition [32], [33]. However, geometric distortion and inconsistency of location coordinates are still found in LA3 imagery. Additional geometric corrections need to be made to ensure the image has an actual location consistent with the standard coordinate system reference. Geometric corrections are required to pre-process remote sensing data and eliminate geometric problems [29], [34]. Geometrically corrected images will remove the spatial distortion give an accurate distance [30]. In this study, further geometric corrections were carried out. The level of geometric correction for LA3 data is rectification. Rectification or geo-reference is the alignment of the image on a map which allows the image to be planimetric. The LA3 image was corrected using the Image-to-Map geographic correction technique. This technique uses a reference map with the Universal Transverse Mercator (UTM) standard reference image [31].

To determine the appropriate band composite in detecting oil spills this study uses the Optimum Index Factor (OIF) calculation. The highest value of OIF calculation indicates the appropriate band composite to distinguish oil spills in the sea. The number of band combinations was calculated using the following factorial equation:

$$\binom{N}{3} = \frac{N!}{(3!(N-3)!)}$$

where:

N = Total number of bands in the satellite list

Then OIF calculation is obtained from the statistical extraction results of the training area covering the oil spill objects. The OIF calculation in this study used four bands of the LA3 satellite, namely bands 1-4. It covers visible light (red, green, blue) and Near-Infrared (NIR). The OIF algorithm uses the total value of standard deviations divided by the correlation coefficient of the bands selected as follows the formula [36], [37]:

$$OIF = \sum_{i=1}^3 SD_i / \sum_{j=1}^3 ABS(CC_j)$$

Where:

SDi = Standard deviation of a band i

ABS = Absolute value of 3-band correlation coefficient

E. Satellite Image Processing

The oil spill occurrence is studied by developing false-color composites (FCC) according to the OIF calculation result. The oil spill features can be revealed by displaying different color composites through the multispectral image, and it will optimize the differentiation of certain specific features of the observed object [38]. Four composite color

combinations are developed in RGB format and visually interpreted.

Remote sensing satellite images are generally stored in digital form, where a two-dimensional image is displayed on a computer screen as a set of discrete digital numbers. Each pixel in the image has a digital number according to the level of brightness or grey level [25]. Digital Number (DN) extraction is intended to determine the characteristics of oil in LA3 based on the value for each pixel. SNAP software was used for this extraction. Each band is viewed in a profile graph by creating a water-oil-water line. Then, the DN information and path in pixels appeared.

F. Post-Processing

A post-processing process is a visual interpretation by visually observing oil spills on the image in detail. An oil spill on the image is observed by paying attention to the patterns formed and the difference of color object (rather oil spill) on the sea surface. In this stage, a combination of bands in LA3 image is examined to obtain a contrast difference in oil spill object with other objects around them. This study is using Sentinel-2 image to do validation of oil spill features on LA3 image, whereas the selected Sentinel-2 image has been confirmed that the oil spill is recorded.

III. RESULTS AND DISCUSSION

A. Results

1) *OIF Calculation of LAPAN-A3*: This study utilized LAPAN-A3 imagery data and conducted the preliminary detection of oil spill objects using the OIF method to obtain the most powerful combination of bands. Since the LISA sensor in LA3 has only four bands, a Visible-NIR band combination is examined. The highest OIF value can represent the best combination of bands in distinguishing the earth objects on images. The band combinations resulted from the OIF method evaluating the standard deviation of each band and the correlation coefficient among the bands selected.

The result of the OIF calculation indicates that the combination of band 1 (Blue), band 2 (Green), and band 4 (NIR) has the highest value at 839.414 and places this combination in the first rank (Table 2), even though it is a bit different in a number with a combination of band 2,3,4. Whilst, the lowest OIF value belongs to a combination of bands 1,2,3 (Blue-Red-NIR) by 473.661. An interesting part of this result is that the combination of band 1,2,3 (Blue-Green-Red) has the highest correlation coefficient value of bands but only has an OIF value of 559.686. According to Ziliwu et al. [39], the higher the total standard deviation of the three bands used, the more information is generated, while the smaller the total correlation coefficient between the two bands used, the less duplication produced. The optimum combination of three bands with the highest OIF value can have the maximum extraction of the object selected with the least amount of duplication [34]. Refers to the OIF calculation result (Table 2), the band combination with the highest OIF that highlighted spectral range for oil spill detection is band 1,2,4, or Blue-Green-NIR. Further out, this combination of bands is utilized for the next analysis.

TABLE II
OIF VALUES OF LAPAN-A3

Band combinations	Sum of standard deviations	Sum of correlation coefficient of bands	OIF	Rank
124 (Blue-Green-NIR)	1254.08503	1.494	839.414	1
234 (Green-Red-NIR)	1317.27643	1.587	830.042	2
123 (Blue-Green-Red)	1326.45746	2.37	559.686	3
134 (Blue-Red-NIR)	689.17646	1.455	473.661	4

2) *OIL Spill Detection and Analysis*: The appearance of the oil layer on each band combination is different. In the RGB combination, one can see a thin pattern (shown in a red circle) on the surface of the water, but it is not very clear. In this combination, it is doubtful whether this pattern is oil or not. On BGR, two patterns are seen that are clearer than the RGB combination. The combination of GRN showed no pattern, and the combination of BGN showed two patterns again on the water surface. When compared to the BGR combination, the pattern in the BGN combination is clearer.

Band combinations were also performed in the Karawang area. The combination selection is the same as Bintan. As a result, RGB and GRN do not show any patterns. The combination of BGR and BGN shows a pattern (shown in the red arrow). However, BGN is clearer than BGR, and the BGN combination can clearly show the oil rig. Based on these results, a comparison is made between LA3 (BGN combination) and Sentinel-2. For Sentinel-2 using the SNR combination, according to the results of research by Dave, Joshi, and Srivastava [35] regarding the appropriate band combination for Sentinel-2 in detecting oil spills. The comparison results are in Fig. 3.

With the BGN combination on LA3, the oil slick looks reddish on the sea surface, while on Sentinel-2 the SWIR-NIR-Red (SNR) combination shows a greenish pattern (Fig. 3). Hu et al. [4] conducted research with Landsat-8 combination SWIR-NIR-Red showing a greenish and reddish colored pattern. The greenish color has higher reflectance in NIR than SWIR, indicating that the oil is an oil-in-water emulsion. In this emulsion type, the oil phase is the dispersed phase, and water is the dispersion medium [36].

On the other hand, reflectance in SWIR is higher than NIR and will cause a reddish color. This indicates that the reddish pattern is a water-in-oil emulsion oil. This emulsion occurs when the dispersed phase consists of water and oil as a dispersion medium [36]. These emulsions sometimes form after oil is spilled onto the water's surface [37]. When this emulsion is formed, the physical properties of the oil change drastically. Liquids are converted into semi-solid and heavy materials. Oil spill recovery equipment should be used, as these emulsions are difficult to recover. The oil spill incident in Karawang was an event that resulted in a fairly widespread of oil. Therefore, oil is quite easily detected at this location. The appearance of oil on LA3 is brownish and on Sentinel-2 is a dark pattern. The oil layer has a reflectance contrast at 400-700 nm [38]. Sensors with the visible to near-infrared (VNIR) spectral range can recognize the spectral change associated with oil-covered water [39]. Debdi [42] explained that at 400-600 nm (Blue-Green), the bottom disturbance is

minimized and eliminated at 600 nm. The 660 - 760 nm range is the best for detecting oil spills in coastal. Meanwhile, Abdunaser [38] explained that concentrated oil would appear

brownish with a wavelength of 600-700 nm, and if it is close to 700 nm, it will be brownish-red.

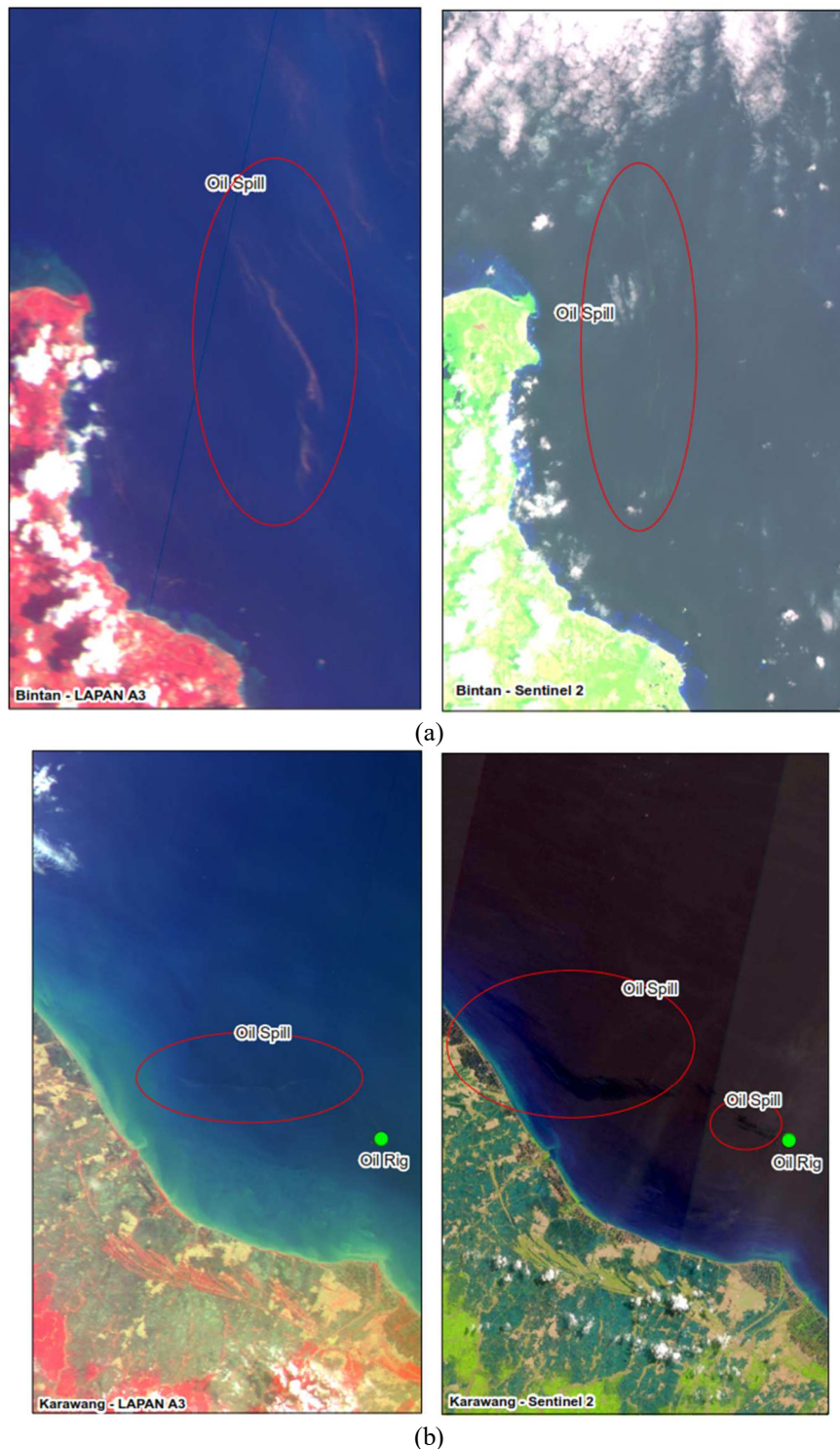


Fig. 3 (a) LA3 (Blue-Green-NIR) and Sentinel-2 (SWIR-NIR-Red) in Bintan; (b) LA3 (Blue-Green-NIR) and Sentinel-2 (SWIR-NIR-Red) on Karawang

Pure oil can be detected in a narrow band of reflection at NIR-SWIR reflectance [43]. At a mixing ratio of oil and water of 60:40, the reflectance of NIR-SWIR also increases with increasing oil thickness. Reflectance of oil emulsions has a greater reflectance as compared to water in the NIR range [3].

The biggest change in NIR reflectance is because the oil is less absorbent at this wavelength [40], [41]. In NIR, the reflectance level and absorption features are caused by organic compounds in the oil that have variations in the thickness of the oil, such as the mixing ratio of oil and water.

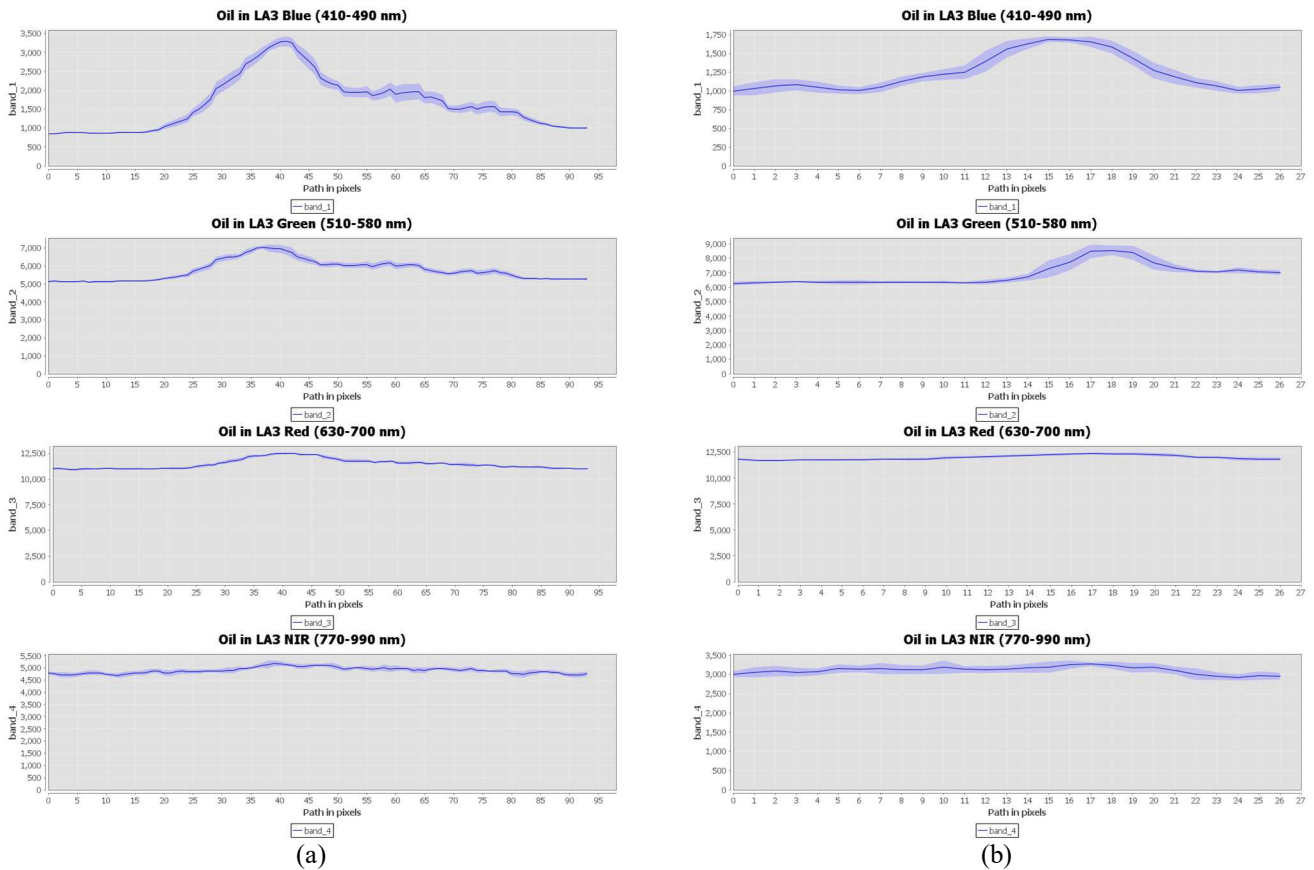


Fig. 4 Histogram of DN value for the Oil Spill and Water Object in each band for (a) Bintan and (b) Karawang. The X-axis is path in pixels and the Y-axis is DN value (Source: Data Processing)

LA3 cannot be further processed for reflectance yet. Previous studies have tried to change the DN to TOA radiance in the Madura region, but further studies need to be done to determine the validity of the resulting coefficient on all images [44], [45]. Therefore, we evaluate DN LA3 in each band both in Bintan and Karawang (Fig. 4). The extraction results show that the Blue and Green bands have prominent peaks in both the Bintan and Karawang areas even though the two areas have different types of oil. This striking pattern is oil. Oil was detected in the range of DN 1,000 to 3,500 for Blue in Bintan and 1,000 to 1,750 for Blue in Karawang. For Green on Bintan, oil was detected in the range of DN 5,000 to 7,000 and in Karawang with a DN value of 6,000 to 8,000. A red band peak in Bintan has been detected, but in Karawang, it is not visible, likewise with NIR.

B. Discussion

This unique property of oil can be studied, especially when it interacts with light and satellite sensors receive it. Oil has a higher emissivity than water, so when it is exposed to sunlight, it emits infrared radiation [19]. The oil layer that is exposed to sunlight will emit infrared radiation. This is the basis for using NIR as a combination band in LA3. The appearance of the oil on the Blue-Green band is unique, making it easier to detect oil spills. The type of oil can be found through optical satellites. Hu et al. [4] noted that the reddish pattern is an oil-in-water emulsion, while the greenish pattern is a water-in-oil emulsion. The oil also contains asphaltene compounds which are very strongly absorbed in Blue and UV, and the tiny

particles in the oil scatter the light and limit the penetration to form a dark reddish color [40].

Meanwhile, the thin oil spill appears in light greenish, fine texture, and wide flow pattern since the thin oil has high reflectance [19]. Thin oil in Sentinel-2 MSI is well detected from the Green to Red bands (543-680 nm), while LA3, which has a resolution similar to Sentinel-2, also produces the same-colored oil appearance as Sentinel-2. In other words, LA3 can detect thin oil spills. However, further research is still needed on the capabilities of LA3, especially field validation.

This difference cannot be separated from the ability of the SWIR band. The SWIR band is important for determining the type of oil and the bonds of organic molecules and compounds. Overtones and combinations of organic molecules and compounds are dominant in petroleum reflectance spectra for NIR-SWIR. Spectral wavelength can be classified for all oils in Table 3 [46]:

TABLE III
CLASSIFIED OIL SPILLS ACCORDING TO SPECTRAL WAVELENGTH

Wavelength (nm)	Group
1390/1410	O-H first overtone and C-H first combinations first overtone
1720-1730	There are found a combination of the CH ₃ and CH ₂ stretching. Also, the combination of symmetric and asymmetric CH ₂ stretching
1750-1760	there is an overtone of the CH ₂ vibration
2310	filled by the combination of the CH ₃ asymmetric axial deformation with the CH ₃ symmetric angular deformation, or a composite of the CH ₃ symmetric axial

2350	deformation with the CH ₃ asymmetric+CH ₂ symmetric angular deformation resulted from the combination of the CH ₃ symmetric axial deformation and the CH ₃ symmetric angular deformation. In general, C-H composite dominates the spectral range between 1950 to 2450 nm
------	--

IV. CONCLUSION

This study assessed the LISA sensor belonging to LA3 to detect the oil spill features in two different causes. The visible and near-infrared spectral range in LA3 was studied for oil spill detection by creating a band composite with FCC (False Color Composite). The proposed method discriminated the oil spill features well. The right band combination can distinguish the features of oil on the sea surface. Blue-Green-NIR is the recommended combination for LA3. LA3 does not have a SWIR band, so it is difficult to determine the type of oil. However, because it is only visible and NIR bands in LA3, it still has limitations in detecting the type and thickness of oil in detail. This study demonstrated the potential use of the LISA sensor in LA3 with the proposed band composite to discriminate and assess the oil spill events. Therefore, LA3 detection is only up to the detection of the presence of oil, not to determine the type of oil.

ACKNOWLEDGMENT

This work is supported by the Research Center for Remote Sensing, National Research and Innovation Agency (BRIN), Jakarta, Indonesia. We thank the Research Center for Satellite Technology, National Research and Innovation Agency (BRIN), Bogor, Indonesia, for providing LA3 data. All authors have different contributions and responsibilities. Pingkan Mayestika Afgatiani and Andi Ibrahim as the main contributors (concept, data processing, data display, analysis data, and writing), while Maryani Hartuti, Ega Asti Anggari, Agus Herawan, Patria Rachman Hakim, and Ety Parwati as member contributors (writing and editing).

REFERENCES

[1] J. Chenhao and X. Yupeng, "Risk Analysis and Emergency Response to Marine Oil Spill Environmental Pollution," *IOP Conf. Ser. Earth Environ. Sci.*, vol. 687, no. 1, 2021, doi: 10.1088/1755-1315/687/1/012070.

[2] P. Klotz, I. R. Schloss, and D. Dumont, "Effects of a chronic oil spill on the planktonic system in San Jorge Gulf, Argentina: a one-vertical-dimension modeling approach," *Oceanography*, vol. 31, no. 4, pp. 81–91, 2018.

[3] B. Zhang, E. J. Matchinski, B. Chen, X. Ye, L. Jing, and K. Lee, *Marine oil spills-oil pollution, sources and effects*, Second Edi. Elsevier Ltd., 2018.

[4] C. Hu, Y. Lu, S. Sun, and Y. Liu, "Optical Remote Sensing of Oil Spills in the Ocean: What Is Really Possible?," *J. Remote Sens.*, vol. 2021, pp. 1–13, 2021, doi: 10.34133/2021/9141902.

[5] S. Sun, Y. Lu, Y. Liu, M. Wang, and C. Hu, "Tracking an Oil Tanker Collision and Spilled Oils in the East China Sea Using Multisensor Day and Night Satellite Imagery," *Geophys. Res. Lett.*, vol. 45, no. 7, pp. 3212–3220, 2018, doi: 10.1002/2018GL077433.

[6] P. Amir-Heidari *et al.*, "A state-of-the-art model for spatial and stochastic oil spill risk assessment: A case study of oil spill from a shipwreck," *Environ. Int.*, vol. 126, no. October 2018, pp. 309–320, 2019, doi: 10.1016/j.envint.2019.02.037.

[7] J. Yang, J. Wan, Y. Ma, J. Zhang, and Y. Hu, "Characterization analysis and identification of common marine oil spill types using hyperspectral remote sensing," *Int. J. Remote Sens.*, vol. 41, no. 18, pp. 7163–7185, 2020, doi: 10.1080/01431161.2020.1754496.

[8] M. Krestenitis, G. Orfanidis, K. Ioannidis, K. Avgerinakis, S. Vrochidis, and I. Kompatsiaris, "Oil spill identification from satellite images using deep neural networks," *Remote Sens.*, vol. 11, no. 15, pp. 1–22, 2019, doi: 10.3390/rs11151762.

[9] J. Chen, W. Zhang, Z. Wan, S. Li, T. Huang, and Y. Fei, "Oil spills from global tankers: Status review and future governance," *J. Clean. Prod.*, vol. 227, pp. 20–32, 2019, doi: 10.1016/j.jclepro.2019.04.020.

[10] R. Al-Ruzouq *et al.*, "Sensors, features, and machine learning for oil spill detection and monitoring: A review," *Remote Sens.*, vol. 12, no. 20, pp. 1–42, 2020, doi: 10.3390/rs12203338.

[11] V. H. R. Prudente, V. S. Martins, D. C. Vieira, N. R. de F. e. Silva, M. Adami, and I. D. A. Sanches, "Limitations of cloud cover for optical remote sensing of agricultural areas across South America," *Remote Sens. Appl. Soc. Environ.*, vol. 20, no. September, p. 100414, 2020, doi: 10.1016/j.rsase.2020.100414.

[12] M. Fingas and C. E. Brown, *Oil Spill Remote Sensing*. Elsevier Inc., 2017.

[13] F. Lei, W. Wang, W. Zhang, K. Li, and Z. Xu, "Oil Spills Tracking Through Texture Analysis from MODIS Imagery," *Int. Geosci. Remote Sens. Symp.*, pp. 9768–9771, 2019, doi: 10.1109/IGARSS.2019.8898595.

[14] T. Lacava *et al.*, "A MODIS-based robust satellite technique (RST) for timely detection of oil spilled areas," *Remote Sens.*, vol. 9, no. 2, pp. 1–15, 2017, doi: 10.3390/rs9020128.

[15] M. S. Ozgizis, J. D. Kaduk, and C. H. Jarvis, "Mapping terrestrial oil spill impact using machine learning random forest and Landsat 8 OLI imagery: a case site within the Niger Delta region of Nigeria," *Environ. Sci. Pollut. Res.*, vol. 26, no. 4, pp. 3621–3635, 2019, doi: 10.1007/s11356-018-3824-y.

[16] N. Arslan, "Assessment of oil spills using Sentinel 1 C-band SAR and Landsat 8 multispectral sensors," *Environ. Monit. Assess.*, vol. 190, no. 11, 2018, doi: 10.1007/s10661-018-7017-4.

[17] P. Kolokoussis and V. Karathanassi, "Oil spill detection and mapping using sentinel 2 imagery," *J. Mar. Sci. Eng.*, vol. 6, no. 1, 2018, doi: 10.3390/jmse6010004.

[18] J. J. A. Althawadi and M. Hashim, "An Approach of Vicarious Calibration of Sentinel-2 Satellite Multispectral Image Based on Spectral Library for Mapping Oil Spills," *Int. Arch. Photogramm. Remote Sens. Spat. Inf. Sci. - ISPRS Arch.*, vol. 42, no. 4/W16, pp. 117–121, 2019, doi: 10.5194/isprs-archives-XLII-4-W16-117-2019.

[19] S. Rajendran *et al.*, "Sentinel-2 image transformation methods for mapping oil spill – A case study with Wakashio oil spill in the Indian Ocean, off Mauritius," *MethodsX*, vol. 8, 2021, doi: 10.1016/j.mex.2021.101327.

[20] W. Hasbi and Suhermanto, "Development of LAPAN-A3/IPB satellite an experimental remote sensing microsatellite," *34th Asian Conf. Remote Sens. 2013, ACRS 2013*, vol. 2, no. October, pp. 1508–1515, 2013.

[21] Z. Zylshal, R. Wirawan, and D. Kushardono, "Assessing the Potential of LAPAN-A3 Data for Landuse/landcover Mapping," *Indones. J. Geogr.*, vol. 50, no. 2, pp. 184–196, 2019, doi: 10.22146/ijg.31449.

[22] Z. Zylshal, "Topographic correction of Lapan-A3/Lapan-IPB multispectral image: A comparison of five different algorithms," *Quaest. Geogr.*, vol. 39, no. 3, pp. 33–45, 2020, doi: 10.2478/quageo-2020-0021.

[23] Z. Zylshal, "Performance evaluation of different DEMs for topographic correction on LAPAN-A3: preliminary results," no. November 2019, p. 1, 2019, doi: 10.1117/12.2543437.

[24] F. Löw, K. Stieglitz, and O. Diemar, "Terrestrial oil spill mapping using satellite earth observation and machine learning: A case study in South Sudan," *J. Environ. Manage.*, vol. 298, 2021, doi: 10.1016/j.jenvman.2021.113424.

[25] A. K. Wijayanto, S. M. Yusuf, and W. A. Pambudi, "The Characteristic of spectral reflectance of LAPAN-IPB (LAPAN-A3) Satellite and Landsat 8 over agricultural area in Probolinggo, East Java," *IOP Conf. Ser. Earth Environ. Sci.*, vol. 284, no. 1, pp. 1–14, 2019, doi: 10.1088/1755-1315/284/1/012004.

[26] A. Herawan, A. Julzarika, P. R. Hakim, and E. A. Anggari, "Object-Based on Land Cover Classification on LAPAN-A3 Satellite Imagery Using Tree Algorithm (Case Study: Rote Island)," *Int. J. Adv. Sci. Eng. Inf. Technol.*, vol. 11, no. 6, pp. 2254–2260, 2021, doi: 10.18517/ijaseit.11.6.14200.

[27] S. Arifin, I. Carolita, and T. Kartika, "Aplikasi model geobiofisik NDVI untuk identifikasi hutan pada data satelit Lapan-A3," *J. Penginderaan Jauh dan Pengolah. Data Citra Digit.*, vol. 16, no. 2, pp. 91–100, 2019.

- [28] N. M. N. Khamsah, S. Utama, R. H. Surayuda, and P. R. Hakim, "The development of LAPAN-A3 satellite off-nadir imaging mission," *Proc. 2019 IEEE Int. Conf. Aerosp. Electron. Remote Sens. Technol. ICARES 2019*, pp. 3–8, 2019, doi: 10.1109/ICARES.2019.8914347.
- [29] D. Traganos and P. Reinartz, "Mapping Mediterranean seagrasses with Sentinel-2 imagery," *Mar. Pollut. Bull.*, vol. 134, no. March, pp. 197–209, 2018, doi: 10.1016/j.marpolbul.2017.06.075.
- [30] P. R. Hakim, A. H. Syafrudin, S. Salaswati, S. Utama, and W. Hasbi, "Development of Systematic Image Preprocessing of LAPAN-A3/IPB Multispectral Images," *Int. J. Adv. Stud. Comput. Sci. Eng.*, vol. 7, no. 10, pp. 9–18, 2019.
- [31] P. R. Hakim, A. H. Syafrudin, A. Wahyudiono, and S. Utama, *Autonomous Band Co-registration of LAPAN-A3 Multispectral Imager using Edge Detection and Fast Fourier Transform*, vol. 2143, no. September. 2017.
- [32] P. R. Hakim, W. Hasbi, and A. H. Syafrudin, "ADCS requirements of Lapan-A3 satellite based on image geometry analysis," *Proceeding - ICARES 2014 2014 IEEE Int. Conf. Aerosp. Electron. Remote Sens. Technol.*, pp. 142–146, 2014, doi: 10.1109/ICARES.2014.7024383.
- [33] M. A. Aguilar, A. Nemmaoui, F. J. Aguilar, A. Novelli, and A. García Lorca, "Improving georeferencing accuracy of Very High Resolution satellite imagery using freely available ancillary data at global coverage," *Int. J. Digit. Earth*, vol. 10, no. 10, pp. 1055–1069, 2017, doi: 10.1080/17538947.2017.1280549.
- [34] A.-M. Loghin, J. Otepka-Schremmer, C. Ressler, and N. Pfeifer, "Improvement of VHR Satellite Image Geometry with High Resolution Elevation Models," *Remote Sens.*, vol. 14, no. 10, p. 2303, 2022, doi: 10.3390/rs14102303.
- [35] C. P. Dave, R. Joshi, and S. S. Srivastava, "A Survey on Geometric Correction of Satellite Imagery," *Int. J. Comput. Appl.*, vol. 116, no. 12, pp. 24–27, 2015, doi: 10.5120/20389-2655.
- [36] T. D. Acharya, I. T. Yang, and D. H. Lee, "Land cover classification of imagery from landsat operational land imager based on optimum index factor," *Sensors Mater.*, vol. 30, no. 8, pp. 1753–1764, 2018, doi: 10.18494/SAM.2018.1866.
- [37] S. R. Yousif and W. F. Shneen, "Using Optimum Index Factor and Determinant Covariance Methods and Compare to PCA on Satellite Images to Determine the Earth's Landmarks (Part of Tar- An Najaf and Its Neighbours)," *J. Phys. Conf. Ser.*, vol. 1660, no. 1, 2020, doi: 10.1088/1742-6596/1660/1/012077.
- [38] K. Abdunaser, "Spatio-temporal analysis of oil lake and oil-polluted surfaces from remote sensing data in one of the Libyan oil fields," *Sci. Rep.*, vol. 10, no. 1, pp. 1–13, 2020, doi: 10.1038/s41598-020-76992-5.
- [39] M. S. Ziliwu, Tulus, Sutarman, M. Zarlis, Z. Situmorang, and A. S. Harahap, "Optimum Index Factor and Cloud Removal on the Landsat Imagery Data Processing," *J. Phys. Conf. Ser.*, vol. 1116, no. 2, 2018, doi: 10.1088/1742-6596/1116/2/022048.
- [40] M. A. Saad, M. Kamil, N. H. Abdurahman, R. M. Yunus, and O. I. Awad, "An overview of recent advances in state-of-the-art techniques in the demulsification of crude oil emulsions," *Processes*, vol. 7, no. 7, pp. 1–26, 2019, doi: 10.3390/pr7070470.
- [41] M. Fingas, "Handbook of Oil Spill Science and Technology," *Handb. Oil Spill Sci. Technol.*, pp. 1–693, 2015, doi: 10.1002/9781118989982.
- [42] B. Debdiip, "Optimum Index Factor (OIF) for Landsat Data: A Case Study on Barasat Town, West Bengal, India," *Int. J. Remote Sens. Geosci.*, vol. 2, no. 5, pp. 11–17, 2013.
- [43] P. M. Afgatiani, F. A. Putri, A. G. Suhadha, and A. Ibrahim, "Determination of Sentinel-2 spectral reflectance to detect oil spill on the sea surface," *Sustinere J. Environ. Sustain.*, vol. 4, no. 3, pp. 144–154, 2020, doi: 10.22515/sustinere.jes.v4i3.115.
- [44] S. Salaswati, P. R. Hakim, A. H. Syafrudin, R. Hartono, and S. Utama, "Vicarious Radiometric Calibration of Lapan-A3 / IPB Satellite Multispectral Imager in Jaddih Hill Madura," *J. Aerosp. Technol.*, pp. 31–42, 2020.
- [45] K. Arai *et al.*, "Method for uncertainty evaluation of vicarious calibration of spaceborne visible to near infrared radiometers," *Int. J. Adv. Comput. Sci. Appl.*, vol. 10, no. 1, pp. 387–393, 2019, doi: 10.14569/IJACSA.2019.0100151.
- [46] T. Lammoglia and C. R. de S. Filho, "Spectroscopic characterization of oils yielded from Brazilian offshore basins: Potential applications of remote sensing," *Remote Sens. Environ.*, vol. 115, no. 10, pp. 2525–2535, 2011, doi: 10.1016/j.rse.2011.04.038.